

# Unraveling the Cellular Mechanism of Assembling Cholesterols for Selective Cancer Cell Death

Huaimin Wang<sup>1</sup>, Zhaoqianqi Feng<sup>1</sup>, Cuihong Yang<sup>2</sup>, Jinjian Liu<sup>2</sup>, Jamie E. Medina<sup>3</sup>, S. Ali Aghvami<sup>4</sup>, Daniela M. Dinulescu<sup>3</sup>, Jianfeng Liu<sup>2</sup>, Seth Fraden<sup>4</sup>, and Bing Xu<sup>1</sup>

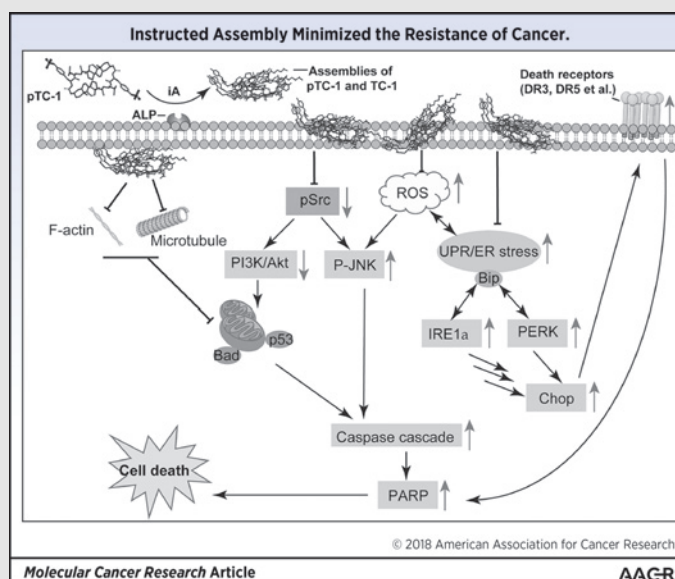


## Abstract

Acquired drug resistance remains a challenge in chemotherapy. Here we show enzymatic, *in situ* assembling of cholesterol derivatives to act as polypharmaceuticals for selectively inducing death of cancer cells via multiple pathways and without inducing acquired drug resistance. A conjugate of tyrosine and cholesterol (TC), formed by enzyme-catalyzed dephosphorylation of phosphorylate TC, self-assembles selectively on or in cancer cells. Acting as polypharmaceuticals, the assemblies of TC augment lipid rafts, aggregate extrinsic cell death receptors (e.g., DR5, CD95, or TRAILR), modulate the expression of oncoproteins (e.g., Src and Akt), disrupt the dynamics of cytoskeletons (e.g., actin filaments or microtubules), induce endoplasmic reticulum stress, and increase the production of reactive oxygen species, thus resulting in cell death and preventing acquired drug resistance. Moreover, the assemblies inhibit the growth of platinum-resistant ovarian cancer tumor in a murine model. This work illustrates the use of instructed assembly (iA) in cellular environment to form polypharmaceuticals *in situ* that not only interact with multiple proteins, but also modulate membrane dynamics for developing novel anticancer therapeutics.

**Implications:** As a multifaceted strategy for controlling cancer cell death, iA minimized acquired resistance of cancer cells, which is a new strategy to amplify the genetic difference between cancer and normal cells and provides a promise for overcoming drug resistance in cancer therapy.

**Visual Overview:** <http://mcr.aacrjournals.org/content/molcanres/17/4/907/F1.large.jpg>.



## Introduction

Tumor cells differ remarkably from their normal cell counterpart due to the longtime oncogenic mutation. The advances

of high-throughput sequencing reveal that tumorigenesis mutations are more numerous and heterogeneous than previously thought (1, 2). Moreover, according to detailed bioinformatics analyses (3), cancer-related driver mutations influence a dozen or more core signaling pathways and processes that are responsible for tumorigenesis. These findings raised the questions about the usefulness of targeting individual signaling molecules as a practical therapeutic strategy. To date, various synthetic- and natural-derived anticancer drugs, with different or similar modes of action, have entered clinical cancer therapy (4). The problem of selectivity and acquired drug resistance, however, remains a challenge. Despite the exciting developments, many cancers still are unresponsive to immunotherapy (5). Thus, there is a need of novel strategies for combating cancers. An emerging concept to address that need is polypharmacology, which aims to develop multitarget drugs (6), that is, a therapeutic agent that interacts with more than one

<sup>1</sup>Department of Chemistry, Brandeis University, Waltham, Massachusetts.

<sup>2</sup>Chinese Academy of Medical Science & Peking Union Medical College, Tianjin, China. <sup>3</sup>Department of Pathology, Brigham and Women's Hospital, Harvard Medical School, Boston, Massachusetts. <sup>4</sup>Department of Physics, Brandeis University, Waltham, Massachusetts.

**Note:** Supplementary data for this article are available at Molecular Cancer Research Online (<http://mcr.aacrjournals.org/>).

**Corresponding Author:** Bing Xu, Brandeis University, 415 South St, Waltham, MA 02454. Phone: 781-736-5201; Fax: 781-736-2516; E-mail: bxu@brandeis.edu

doi: 10.1158/1541-7786.MCR-18-0931

©2018 American Association for Cancer Research.

target or carries out more than one function. In fact, it is rather common for endogenous molecules, small bioactive molecules, or macromolecules, to exhibit multiple functions that are context dependent. One of most notable multifunctional small molecules is cholesterol, which plays an indispensable role in modulating cell signaling transduction and maintains cell membrane hemostasis in mammalian cells (7). The dynamic clustering of cholesterol and sphingolipids forms raft-like structures, which function as a platform for tuning the dynamics of membrane proteins and signal transduction (8). Recent studies also unveiled important approaches that target plasma membrane for modulating immune cell signaling to enhance immune response against cancer cells (9). These advancements support the exploration of therapeutics outside the domain of tight ligand–receptor or antibody–antigen interactions.

To explore outside the dogma of ligand–receptor binding, we have been developing instructed assembly (iA) of small molecules for generating higher order structures in cellular environment, which exhibits exciting promises in cancer therapy or imaging (10–12). Our recent finding revealed that pericellular assemblies instructed by GPI-anchored ectoenzymes (e.g., alkaline phosphatases; ref. 13) on cell membrane selectively induce cancer cell death (14). To reduce the dosage for satisfying clinical needs, we developed a cholesterol derivative (phosphorylate TC, **pTC-1**) as the molecules for iA. Our results indicate that **pTC-1** exhibits excellent potency against platinum-resistant ovarian cancer cells (15). Previous results of solid NMR indicated that **pTC-1** transformed to **TC-1** in the presence of phosphatase. We also have found that uncompetitive inhibitors of phosphatase in cells rescue cells from exposure to **pTC-1**, and dephosphorylation of **pTC-1** by exogenous ALP abolish the cytotoxicity of **pTC-1** (15). These results together suggested the importance of iA for inducing cell death. The precise cellular mechanism of the selective cancer cell death resulting from the iA of **pTC-1**, however, remains to be elucidated, and the *in vivo* efficacy of iA of **pTC-1** is yet to be examined.

In this work, using various biochemical methods, we show that enzymatically controlled *in situ* assemblies of the cholesterol derivative acts as polypharmaceuticals for selectively inducing death of cancer cells via multiple death pathways and without resulting in acquired drug resistance. Specifically, **pTC-1** is able to form assemblies of **TC-1** (after dephosphorylation) selectively on or in cancer cells (Fig. 7, Visual Overview). The assemblies of **TC-1** augment lipid rafts, aggregate extrinsic cell death receptors (e.g., DR5, CD95 or TRAILR), decrease the expression of oncoproteins (e.g., Src and Akt), disrupt the dynamics of cytoskeletons (e.g., actin filaments or microtubules), induce endoplasmic reticulum (ER) stress, and increase the production of reactive oxygen species (ROS), thus resulting in cell death and minimizing acquired drug resistance. Moreover, xenograft mouse model demonstrates that intraperitoneal injection of **pTC-1** inhibits the growth of the tumor of platinum-resistant ovarian cancer, confirming that iA of **pTC-1** is effective *in vivo*. This study illustrates a new approach for designing iA that utilizes essential, endogenous enzymes to spatiotemporally modulate membranes and proteins for multitargeting and regulating cell behavior, which promises a potential approach to advance anticancer nanomedicines, overcome cancer drug resistance, and complement with immunotherapy.

## Materials and Methods

### Reagents

HeLa, Saos-2, HS-5, HepG2, T98G, and A2780 cells were purchased from ATCC, A2780cis cell from Sigma, and Kuramochi and OVSAHO cell lines from the Dinulescu laboratory at Harvard Medical School (Boston, MA). DMEM, McCoy 5A medium, and RPMI1640 medium were purchased from ATCC, and FBS and penicillin/streptomycin from Gibco by Life Technologies. 3-(4,5-Dimethylthiazol-2-yl)-2,5-diphenyltetrazolium bromide (MTT) was purchased from ACROS Organics, ER Stress Antibody Kit from Cell Signaling Technology, and other antibodies from Abcam.

### Cell culture

HeLa, T98G, HepG-2, HS-5, and Saos-2 cell lines were purchased from ATCC between 2010 and 2017. A2780cis cells were obtained from Sigma-Aldrich in 2016. Kuramochi and OVSAHO were kindly provided by Prof. Dinulescu (Harvard Medical School, Boston, MA). All cell lines were authenticated using short tandem repeat DNA fingerprinting. A2780cis cells were cultured in RPMI1640 medium supplemented with 10% volume for volume (v/v) FBS, 100 U/mL penicillin, and 100 µg/mL streptomycin (cisplatin only necessary every 2–3 passages). HeLa cells, T98G, and HepG-2 cells were cultured in minimum essential medium supplemented with 10% v/v FBS, 100 U/mL penicillin, and 100 µg/mL streptomycin. HS-5 cells were cultured in DMEM supplemented with 10% v/v FBS, 100 U/mL penicillin, and 100 µg/mL streptomycin. Saos-2 cells were cultured in McCoy 5A medium (for Saos-2) supplemented with 15% v/v FBS, 100 U/mL penicillin, and 100 µg/mL streptomycin. Kuramochi and OVSAHO cell lines were cultured in RPMI1640 medium with 10% FBS and 1% penicillin/streptomycin. All cells were incubated at 37°C in a humidified atmosphere of 5% CO<sub>2</sub>.

### MTT assay

All different cell lines were seeded in 96-well plates at  $1 \times 10^5$  cells/well for 24 hours followed by culture medium removal and the subsequent addition of culture medium containing different amounts of the precursors. At designated time (24/48/72 hours), we added 10 µL MTT solution (5 mg/mL) to each well and incubated at 37°C for another 4 hours, and then 100 µL of SDS-HCl solution was added to stop the reduction reaction and to dissolve the purple formazan. The absorbance of each well at 595 nm was measured by a multimode microplate reader. The cytotoxicity assay was performed three times, and the average value of the three measurements was taken.

### Actin staining

Cells in exponential growth phase were seeded in a confocal dish (3.5 cm) at  $1.5 \times 10^5$  cells per dish and allowed to fully attach to the culture dish bottom. After removing the culture medium, we added fresh medium containing the test compound. At designated time, we removed the medium and washed with PBS three times, fixed with 4% paraformaldehyde for 15 minutes, and then added 1 mL of 0.1% Triton X-100 in PBS buffer for 30 minutes. After washing the cells three times by PBS, we added 1 mL of 0.1% BSA in PBS 30 minutes, and then washed the cells by PBS three times. PBS (1 mL) containing 5 units of Alexa 633 was added to the cells for 1 hour. After removing the buffer and washing the

cells three times by PBS, we added 1 mL of Hoechst (1  $\mu\text{g/mL}$ ) for 10 minutes. Then, the cells were washed three times with PBS buffer before imaging.

#### Time-dependent Western blot analysis

Cells in exponential growth phase were seeded in 10-cm culture dish and allowed to fully attach to the culture dish bottom. Upon 70% to 80% confluences, we treated cells with the different compounds at different concentrations for times ranging from 0 to 24 hours. After the cells were washed by cold PBS buffer five times, we added cell lysis buffer to the plate for 5 minutes and then the cells were scraped. The lysate solution was transferred into a 1.5 mL Eppendorf tube. After centrifugation of the sample for 20 minutes at  $12,000 \times g$  in a cold microfuge, the supernatant was collected for quantifying the protein concentration by Pierce Coomassie Plus (Bradford) Assay Kit. Loading sample (20  $\mu\text{L}$ ) with SDS loading buffer was added in each lane for SDS-PAGE and Western blot analysis. After boiling the loading samples at  $100^\circ\text{C}$  for 5 minutes, equal amounts of loading sample (20  $\mu\text{L}$ ) were separated using SDS-PAGE in TGS buffer and transferred to polyvinylidene difluoride membranes. After blocking with TBST (TBS with 0.1% Tween 20) containing 5% BSA for 1 hour, the membranes were incubated with the primary antibodies at  $4^\circ\text{C}$  in TBST buffer containing 5% BSA overnight. After washing the membrane five times by TBST, we incubated the membrane with horseradish peroxidase-conjugated goat anti-rabbit IgG antibodies in TBST buffer for 1 hour at room temperature. After washing with TBST five times, the blots were visualized with the Pierce ECL plus Western blotting substrate.

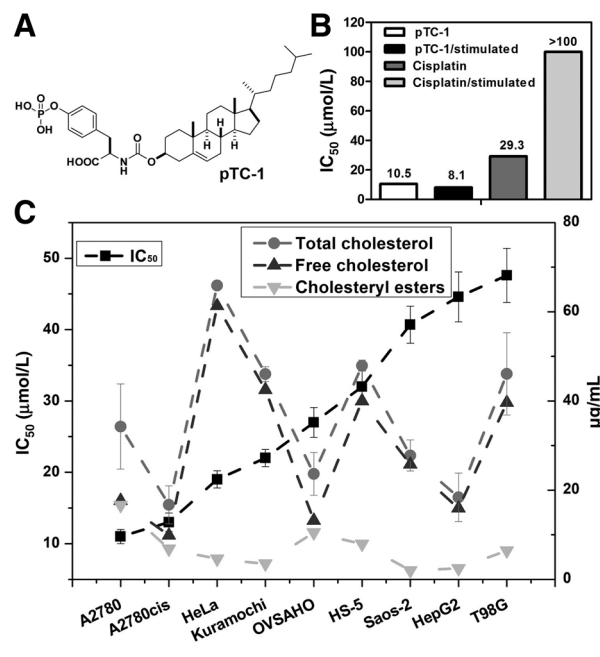
#### In vivo evaluation of antitumor activity

All studies involving animals were approved by The Animal Care and Use Committee of IRM-CAMS. Female Balb/c mice were inoculated with  $2 \times 10^5$  A2780cis cells in the mammary fat pad. Tumor growth was monitored every other day. Tumor volume was calculated by the formula: length  $\times$  width  $\times$  (length + width)/2. After tumor size reached approximately  $50 \text{ mm}^3$ , mice were randomly divided into different treatment groups ( $n = 6$ ). The day of giving compound was designated as day 0 and the compound was given every 2 days. Mice weight was monitored after receiving treatment and presented as relative weight (%).

## Results

#### Inhibition of multiple cancer cell lines

Acquired drug resistance is a major reason that makes chemotherapy ineffective. Our previous results indicate that pTC-1 (Fig. 1A) inhibits the growth of cisplatin-resistant human ovarian cancer cell lines (A2780cis). We also confirmed that pTC-1 selectively inhibits ovarian cancer cells over normal cells (15). To evaluate whether pTC-1 induces acquired resistance, we used the parent, cisplatin-sensitive A2780 cell line to incubate with pTC-1 by gradually increasing concentrations of pTC-1, similar to the method used to induce cisplatin-resistant ovarian cancer cell lines (16). As a control, we also cultured A2780 cell lines with cisplatin. After the treatment of A2780 cell lines by pTC-1 (or cisplatin) for 5 weeks, we tested these stimulated A2780 cells with pTC-1 or cisplatin by MTT assay. As shown in Fig. 1B and Supplementary Fig. S1, the  $\text{IC}_{50}$  of pTC-1 against A2780 cells

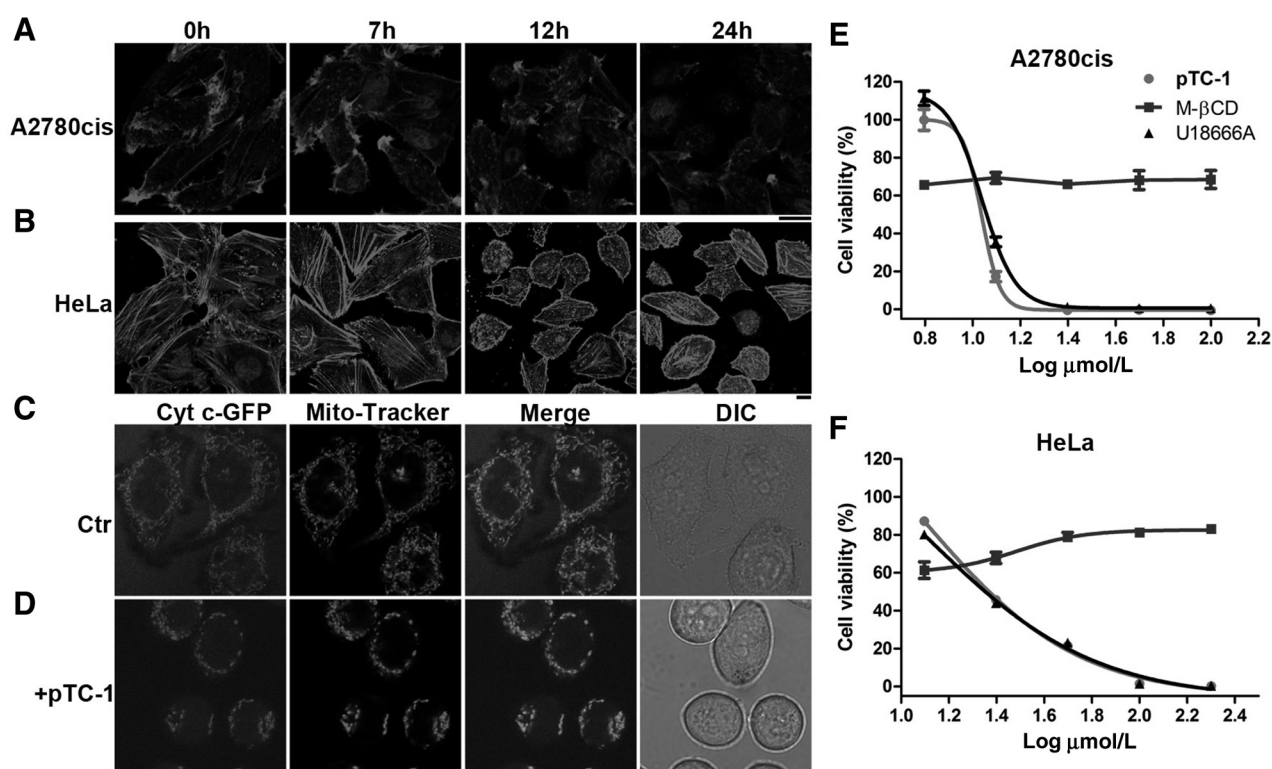


**Figure 1.**

Cytotoxicity of phosphotyrosine cholesterol (pTC-1) and the selective inhibition of multiple cancer cells. **A**, Molecular structure of pTC-1. **B**, Forty-eight hours  $\text{IC}_{50}$  of pTC-1 against unstimulated A2780 cell line or stimulated A2780 cell line (after 5 weeks treatment of the precursors with gradual increase in concentrations). **C**,  $\text{IC}_{50}$  of pTC-1 against different cell lines for 48 hours and the cholesterol contents of different cell lines.

(after 5 weeks stimulation of pTC-1) is 8.1  $\mu\text{mol/L}$  for 48 hours, which is similar with the cytotoxicity of the pTC-1 on the unstimulated A2780 cells (10.5  $\mu\text{mol/L}$ ). On the contrary, the  $\text{IC}_{50}$  of cisplatin is more than 100  $\mu\text{mol/L}$  against A2780 cells (after 5 weeks stimulation of cisplatin), which is much higher than the  $\text{IC}_{50}$  of cisplatin against unstimulated A2780 cells (29.3  $\mu\text{mol/L}$ ).

We next examined the effects of pTC-1 on the viability of cultured cancer cells and normal cells (Fig. 1C; Supplementary Fig. S2). pTC-1 treatment markedly induces cell death in ovarian cancer cells, including two high-grade serous ovarian cancer cell lines, Kuramochi cells and OVSAHO cells. The  $\text{IC}_{50}$  is 22  $\mu\text{mol/L}$  for Kuramochi cells and 27  $\mu\text{mol/L}$  for OVSAHO cells, which is about two times higher than its  $\text{IC}_{50}$  values against cisplatin-sensitive A2780 cells (10.5  $\mu\text{mol/L}$ ) and cisplatin-resistant A2780cis cells (13  $\mu\text{mol/L}$ ). After being incubated with adenocarcinoma (HeLa), pTC-1 exhibits  $\text{IC}_{50}$  of 19  $\mu\text{mol/L}$ , which is comparable with its  $\text{IC}_{50}$  against ovarian cancer cells. In contrast, pTC-1 shows less efficacy against human bone marrow stromal cells (HS-5,  $\text{IC}_{50}$  is 32  $\mu\text{mol/L}$ ) and human osteosarcoma cancer cells (Saos-2, 40.7  $\mu\text{mol/L}$ ), respectively. In addition, the incubation of pTC-1 with hepatocellular carcinoma cells (HepG2) and glioblastoma cancer cells (T98G) results in the  $\text{IC}_{50}$  values at 45 and 48  $\mu\text{mol/L}$ , respectively. The cholesterol contents or cholesteryl ester contents of different cells (Fig. 1C) hardly correlate with the cytotoxicity of pTC-1 on different cell types, further indicating that the cell death induced by pTC-1 is rather resulted from the process of iA than depends on the amount of cholesterol in different types of cells.

**Figure 2.**

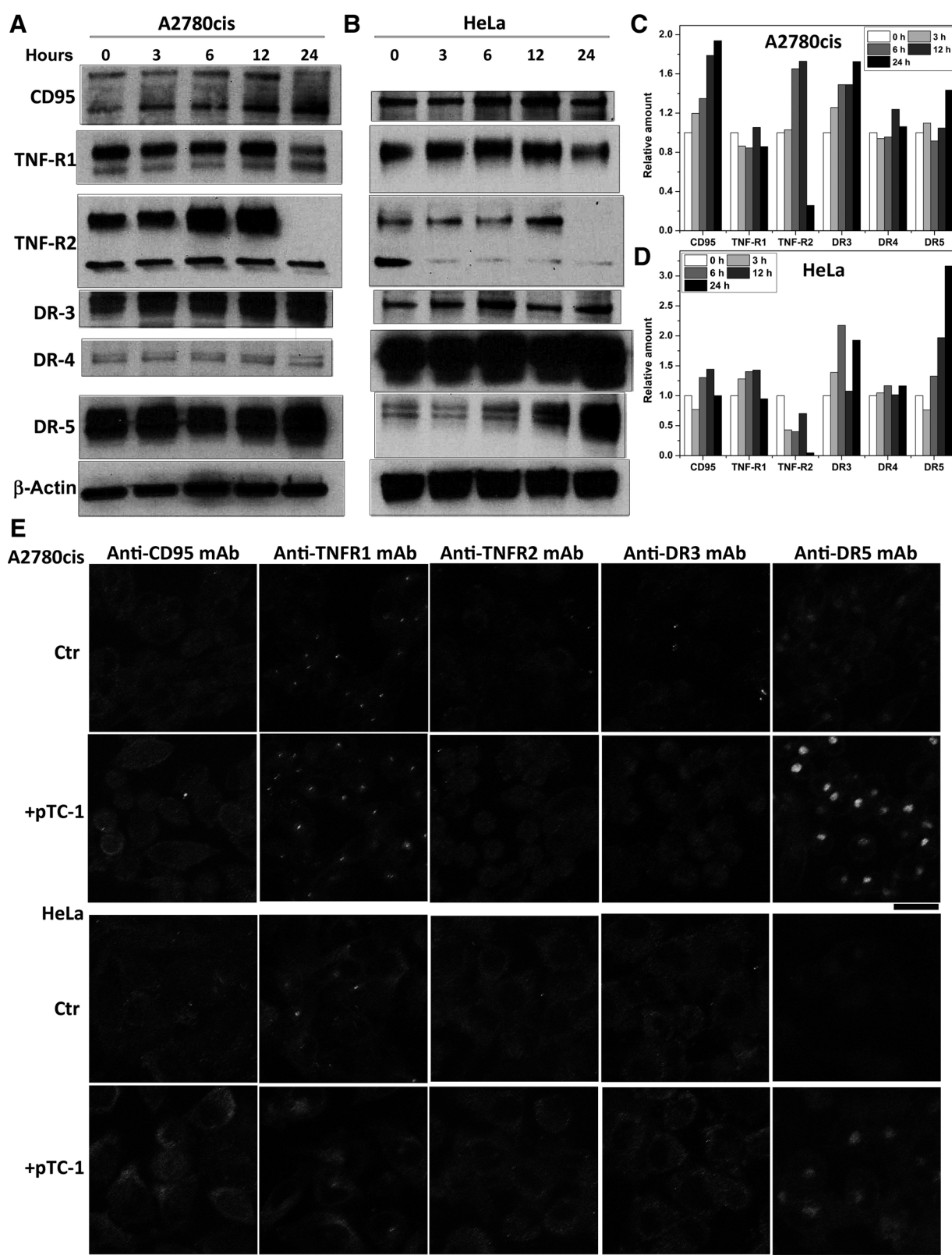
pTC-1 interacts with cell cytoskeleton and induces mitochondria fission. After incubating pTC-1 with A2780cis (A) or HeLa cells (B) to reach designated time points, we used Alexa Fluor 633 phalloidin (F-actin, red) to reveal the changes of actin filaments. The concentration of pTC-1 is 12.5  $\mu\text{mol/L}$  for A2780cis cell and 25  $\mu\text{mol/L}$  for HeLa cell. C and D, pTC-1 (25  $\mu\text{mol/L}$ )-induced fragmental mitochondria in 2H18 HeLa cells (expressing GFP labeled Cyt c). After treating 2H18 HeLa cells for 22 hours by pTC-1, we also used Mito-Tracker (red) to stain cellular mitochondria. Forty-eight hours cell viability of A2780cis (E) or HeLa (F) without or with addition of M- $\beta$ CD and U18666A. The concentrations of M- $\beta$ CD for treating A2780cis and HeLa cells are 5 and 2 mmol/L, respectively. The concentration of U18666A for treating A2780cis and HeLa cell is 1  $\mu\text{g/mL}$ . Scale bar in A-D is 10  $\mu\text{m}$ .

### Disturbing actin dynamics and mitochondrial fusion and fission

An autophagy inhibitor, methyladenine (2 or 5 mmol/L), hardly rescued both A2780cis and HeLa cells treated with pTC-1 (Supplementary Fig. S3), indicating that the cell death induced by pTC-1 unlikely involved autophagy. Moreover, Annexin V-FITC Apoptosis/PI staining suggested that most of cells treated by pTC-1 are early apoptotic cells, which shows green fluorescence, few of the cells were necrotic cells (Supplementary Fig. S4). Actin filaments, as part of cytoskeleton, are critical for variety of cellular processes, including cell growth, division, motility, as well as apoptosis. Previously, we found that *in situ* self-assembly of small molecules on cell surface led to disruption of actin filaments (14, 15). Being treated with NBD-pTC-1, an analogue of pTC-1, A2780cis and HeLa cells exhibited bright fluorescence on cell surface and some fluorescent puncta inside cytoplasm (Supplementary Fig. S5) after 1-hour incubation of the cells with the probes. In addition, more fluorescence appeared inside cells after 5-hour incubation. These results confirm that the enzymatic assemblies form on the cell surface and in the cells. To gain more insights into the dynamics of globular and filamentous actin equilibrium in the presence of pTC-1, we used Alexa Fluor 633 Phalloidin to stain actin filament of A2780cis or HeLa cells that were incubated with pTC-1 for different durations. We chose A2780 cells to examine the acquired drug resistance of pTC-1

(with cisplatin as the reference). We chose HeLa cells because it is a cell line that has served as a model of human cell biology for decades. As shown in Fig. 2A, with the increase of incubation time, the actin filaments start to shrink and become much shorter after the treatment of pTC-1 in both A2780cis and HeLa cells. Without the addition of pTC-1, actin filaments in A2780cis cells exhibit long and fibrous structures and high density at the cell boundary. In contrast, after the cells being incubated with pTC-1 for 7 hours, actin filaments in the cells exist as short fibers or aggregates. After being incubated with pTC-1 for 12 hours, the cells produce more short aggregates of actin filaments. The brighter fluorescence originated from the staining of actin filaments at the cell boundary becomes weaker, and the sizes of the cells start to shrink. Twenty-four hours after the treatment of pTC-1, there are only irregular, short, and dot-like structures of actin aggregates. The change of actin filaments in HeLa cells slightly differs from that in A2780cis cells. The actin filaments at the boundary of cells become denser, and the inner actin filaments become shorter after the treatment of pTC-1 for 7 hours. With the increase of time, actin filaments appear as dots (12 hours) and the cells shrink. This phenomenon lasts for 24 hours, accompanied by some of cells to exhibit apoptotic morphology.

Mutation in actin or actin-binding proteins can influence apoptotic pathways in mitochondria, as revealed by recent reports (17, 18). Chen and colleagues demonstrated that mitochondrial

**Figure 3.**

pTC-1 affects the expression of death receptors. Western blot analysis indicates that the expression level changes relative amounts of cell death receptors upon the treatment of pTC-1 A2780cis (**A**) and HeLa (**B**) cell lines. The quantification of expression level of cell death receptors from Western blot analysis in A2780cis (**C**) and HeLa (**D**) cell lines. **E**, IF shows the changes of cell death receptors without or with the treatment of pTC-1 in A2780cis or HeLa cell lines for 24 hours.

dysfunctions induced by ALA-PDT results in reorganization of cytoskeleton, alternating cellular morphology, and cellular adhesion (18). These findings together indicate that the interaction between actin and mitochondria contribute to cell death. Moreover, fragmented mitochondria is one of the early signs of activation of apoptosis (19). On the basis of these facts and the influences of pTC-1 on cytoskeleton, we examine how the iA of pTC-1 affects the morphology of mitochondria. Using a cell line that has a mitochondrial protein (Cytochrome c) tagged by GFP (20), we monitored the changes of mitochondria during the early stage of cell death after the treatment of pTC-1. After the cells were incubated with pTC-1 for 22 hours, typical tubular mitochondrial structure of healthy cells (Fig. 2C) disintegrated into small, spherical organelles (Fig. 2D), suggesting that pTC-1 results in fragmental mitochondria. To further investigate the contribution of iA of pTC-1, we also examined the effect of methyl- $\beta$ -cyclodextrin (M- $\beta$ CD) and U18666A on the viability of the cells incubated with pTC-1. The former disrupts lipid rafts by removing cholesterol from membranes, and the latter is a well-known intracellular cholesterol transport inhibitor (21). As shown in Fig. 2E and F; Supplementary Fig. S6, M- $\beta$ CD significantly protects the cells, rescuing both A2780cis and HeLa cells at high concentration of pTC-1. In contrast, U18666A slightly increases the viability of the A2780cis cells, but exhibits little protective effect on the HeLa cells, suggesting that the iA of pTC-1 plays a critical role for inducing cell death.

#### Cell death involves extrinsic death pathways

To determine the signaling pathways that are involved in pTC-1-caused cell death, we first determined the effects of pTC-1 on extrinsic death pathways, which play important roles in various biological processes (22). Time-dependent Western blot analysis (Fig. 3A and C; Supplementary Fig. S7) indicates that continuous incubation with pTC-1 induces the increase of the expression levels of CD95, DR3, and DR5 in A2780cis cell lines, while the expression levels of TNF-R1 and DR4 remain almost constant with the treatment of pTC-1 within 24 hours. The changes of these

death receptors slightly differ in HeLa cells (Fig. 3B and D; Supplementary Fig. S7), which express higher levels of DR3 and DR5. Two major bands of CD95 in A2780cis cells represent two forms of CD95, likely due to posttranslational modifications that are ubiquitous in mammalian cells (23).

We also used immunofluorescence (IF) to investigate the changes of other extrinsic death receptors after the treatment of pTC-1. As shown in Fig. 3E, the treatment of pTC-1 increases the expression levels of CD95, TNF-R1, and DR5. This observation is consistent with the results of Western blot analysis. Notably, IF indicates that DR5 colocalizes with the Golgi marker RCAS1 (Supplementary Fig. S8) and exhibits weak fluorescence on cell surface or other organelles, indicating that the activation of DR5 is ligand-independent intracellular activation (24).

#### ER stress for cell death

Recent finding have suggested that upregulation of DR5, as the critical step for ER stress, induces death of several human cancer cells after the treatment of thapsigargin (25, 26). Ashkenazi and colleagues also reported that DR5 integrates opposing unfolded protein response (UPR) signals to control ER stress-induced apoptosis (24, 27). Moreover, ER is the harbor of cholesterol, which traffics from late endosomes. The overburden of cholesterol accumulation in the ER likely contributes to macrophage apoptosis (28). Inspired by these works, and considering that pTC-1 induces expression of DR5 during cell death, we evaluated the change of major ER stress markers in both A2780cis and HeLa cells incubated with pTC-1. Time-dependent Western blot analysis shows that the expression levels of Chop, Bip, and PDI, the indicators of cells under ER stress, increase after the treatment of pTC-1, indicating the induction of ER stress. In addition, our results indicate that pTC-1-induced ER stress also activates IRE1 $\alpha$  branch of UPR, which is the first identified key player in UPR and plays an essential role in protecting cells against lethal consequences of ER stress (26).

Recent studies suggested that oxidative stress is one of the mechanisms involved in Chop-induced cell apoptosis. Our results suggest that iA of pTC-1 generates cytotoxic ROS

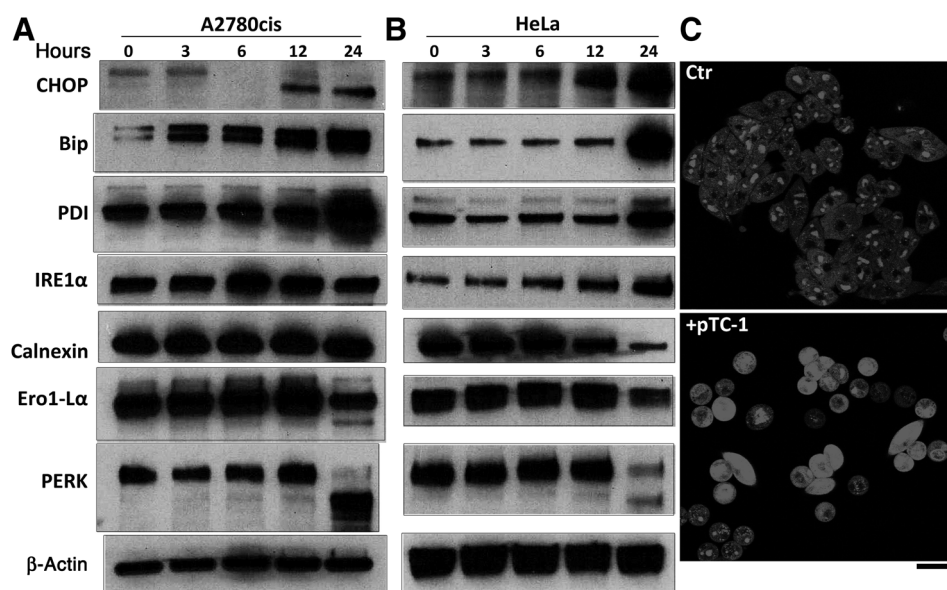


**Figure 4.** pTC-1 induces cell apoptosis via ER stress and generates ROS. Western blot analysis indicates the changes of the expression of ER stress markers in A2780cis (A) and HeLa (B) cell lines upon the treatment of pTC-1. C, CLSM images showing the generation of ROS as measured by dihydroethidium (DHE,  $\lambda_{exc} = 543$  nm, emission was detected at 575–625 nm) in A2780cis without and with treatment with pTC-1 (12.5  $\mu$ mol/L) for 12 hours.

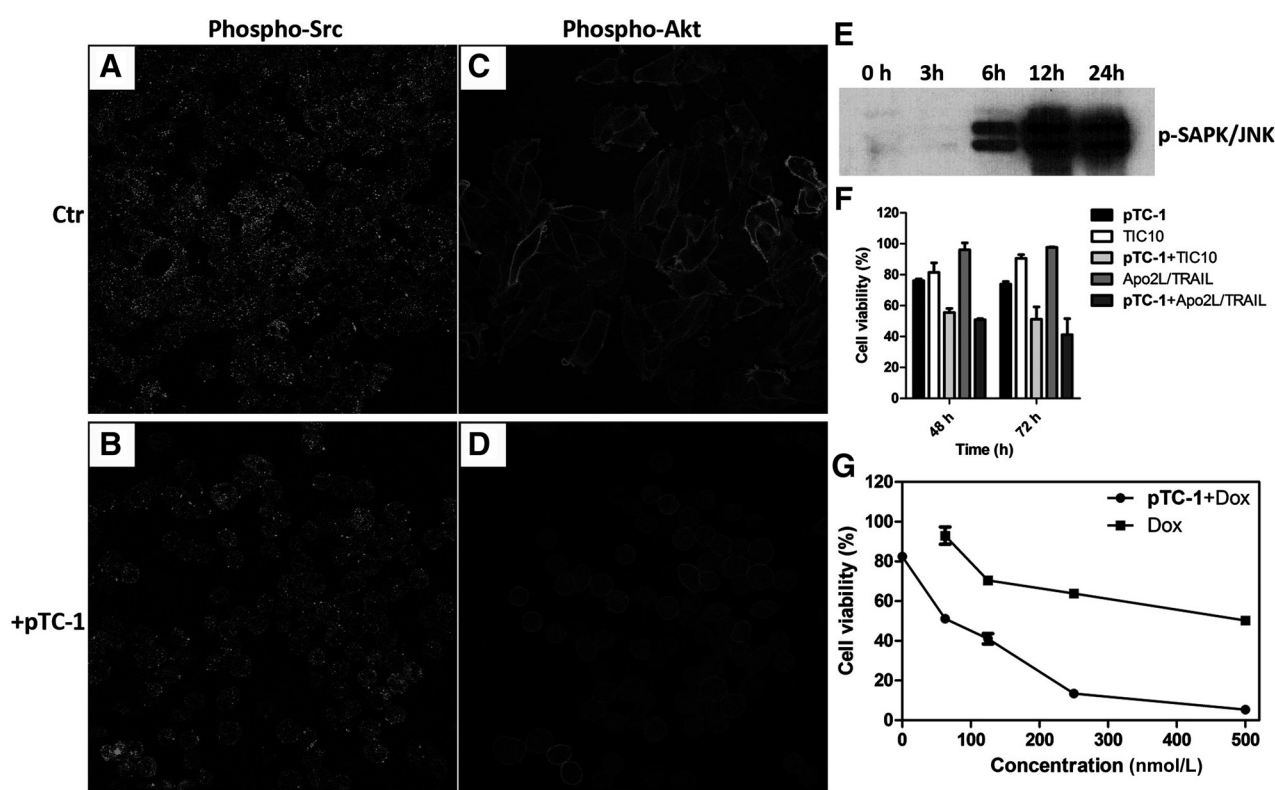


**Figure 5.** pTC-1 decreases the expressions of Src (A and B) and Akt (C and D) in A2780cis cell lines after the treatment of pTC-1 (12.5  $\mu\text{mol/L}$ ) for 24 hours. Scale bar is 25  $\mu\text{m}$ . E, Time-dependent Western blot analysis shows the expression levels of p-SAPK/JNK in A2780cis cell lines. pTC-1 (8  $\mu\text{mol/L}$ ) enhances the effect of different anticancer agents: TIC 10 (5  $\mu\text{mol/L}$ ) and Apo2L/TRAIL (50 ng/mL) (F) and doxorubicin (G) at different concentrations.

(Fig. 4C) in the cell cytoplasm, agreeing with the report that prolonged ER stress hyperoxidizes the ER lumen, resulting in  $\text{H}_2\text{O}_2$  leakage into the cytoplasm and inducing ROS generation in the cytoplasm (26). The oxidation environment of ER lumen is induced by Ero1 $\alpha$  (Fig. 4A), which hyperoxidizes the ER and promotes cell death. Similar to IRE1 $\alpha$ , another branch of UPR is the activation of PERK (29, 30), which is the major protein for attenuating of mRNA translation under ER stress and preventing newly synthesized protein influx into already stressed ER lumen. Our result indicates that PERK activity slightly increases at first 12 hours and decreases by 24 hours.

Calnexin is another molecular chaperone of ER, which plays an essential role for assisting membrane protein folding. Recent studies demonstrated that the expression levels of calnexin and its association with Bap31 partially contribute cancer cell resistance to apoptosis induced by ER stress (31). Being treated with pTC-1, the expression level of calnexin slightly decreases in A2780cis cells and significantly decreases in HeLa cells. In the A2780cis cells treated with pTC-1 for 24 hours, we also found an additional band of calnexin, the product from the calnexin cleaved by caspase-3 or caspase-7. This result agrees with the report that calnexin is cleaved during apoptosis, as well as under ER stress (32). Together with expression levels of these ER markers under normal conditions (Supplementary Fig. S9), these results suggest ER stress, induced by pTC-1, as one of the mechanisms contributing to cell death.

#### Inactivating Src/Akt signaling pathway

Src family kinases (SFK) play crucial roles in the tumor development, including cell proliferation, survival, invasion, migration, adhesion, and angiogenesis (33). In fact, most of tumor tissues overexpress or maintain high activation of SFKs (34). Because of the crucial role of Src in many intracellular signaling processes and in cancer progression, inhibitors of SFKs are currently being developed and undergoing clinical testing (35). It is also known that Src overexpresses in ovarian cancer cells and interacts with transmembrane receptor tyrosine kinases at the cell membrane (36). Thus, pTC-1 should affect the expression of Src in A2780cis cells because iA of pTC-1 occurs at cell membrane (Supplementary Fig. S5).

We used IF to determine the effect of pTC-1 on the expression of Src. The results (Fig. 5A and B) indicate that the expression level of phospho-Src decreases upon the treatment of pTC-1, evidenced by the weaker red fluorescence than that in the untreated A2780cis cells. EGFR is another protein that interacts with Src. Being phosphorylated by Src, EGFR forms complex with Src, which is important for tumorigenesis (37). Comparing with untreated A2780cis cells, our results show more green fluorescence on cell surface (Supplementary Fig. S10), indicating that pTC-1 changes the distribution of EGFR. Moreover, the expression levels of phospho-Akt and stress-activated protein kinase/c-Jun N-terminal kinase (SAPK/JNK), the downstream survival signals of Src, decrease after the treatment of pTC-1 (Fig. 5C, D, and E). These

Wang et al.

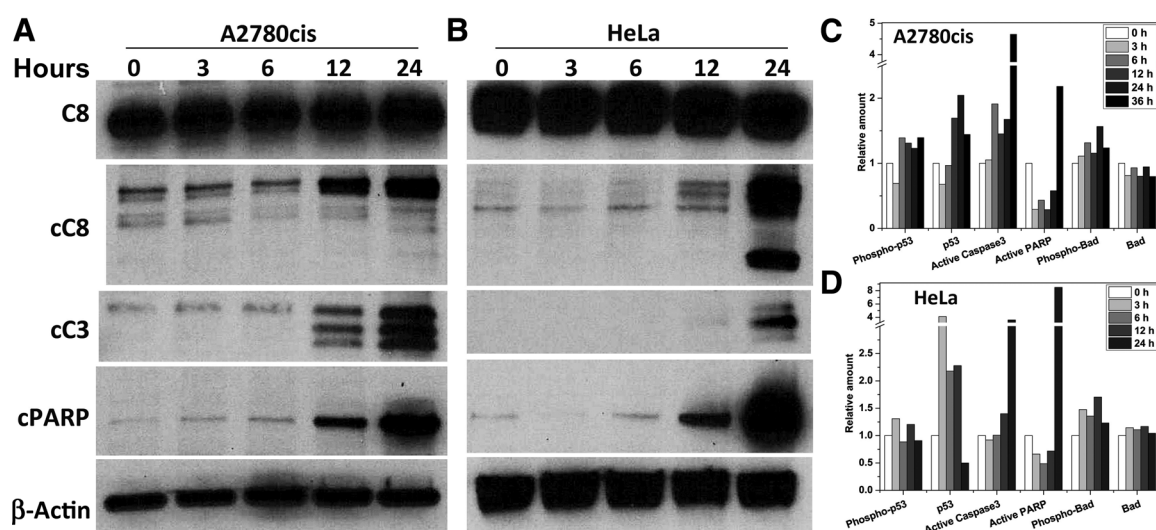


**Figure 6.**

pTC-1 activates the down-stream apoptotic proteins. Time-dependent Western blot analysis shows the expression levels of C8 (caspase-8), cC8 (cleaved caspase-8), cC3 (cleaved caspase-3), and cPARP (cleaved PARP) in A2780cis (A) and HeLa (B) cell lines. Time-dependent ELISA of activation of apoptotic proteins in A2780cis (C) and HeLa (D) cells treated with pTC-1.

results, together, suggest that the Src signaling pathway is involved in the cell death induced by pTC-1. Interestingly, the expression level of JNK also responds to ROS level in cells, which is mediated by IRE1 $\alpha$  (Figs. 4A and 7, and Visual Overview). This observation indicates that iA of pTC-1 results in cross-talk between different cell signaling pathways.

#### Augmenting anticancer efficiency of TRAIL inducer and doxorubicin

Because pTC-1 induces the expression of DR5, the receptor of TRAIL, we expected that pTC-1 would increase the cytotoxicity of TRAIL inducers or cognate ligand. We selected representative TRAIL inducers, TIC10 (38), and soluble cognate ligand, human Apo2L/TRAIL (39), which exhibit potent anticancer efficiency in preclinical trials. Our results indicate that pTC-1, with little cytotoxicity at low concentration (8  $\mu$ mol/L), boosts the cytotoxicity of TIC10 and ApoL/TRAIL (Fig. 5F). Moreover, combination of pTC-1 with doxorubicin, a drug with capacity of sensitizing tumor cells to TRAIL-mediated apoptosis (40), kills A2780cis cells effectively (100 nmol/L of doxorubicin). These results suggest the promise of pTC-1 in combining with clinical drugs for cancer therapy.

#### Cell death via the caspase cascade

To investigate the intrinsic signaling pathways involved in cell death induced by pTC-1, we characterized the changes of the caspase cascade because our previous results indicated that pan-caspase inhibitor z-VAD and PARP inhibitor PJ34 partially rescue cells treated by pTC-1 (15). As shown in Fig. 6A and B, the expression levels of proteolytically cleaved caspase-3, caspase-8, and PARP increase in both A2780cis and HeLa cells, confirming that pTC-1 activates caspase-3 and caspase-8. The activation of these proteins is also measured by ELISA kit in a time-dependent experiment. Caspase-3 and active PARP increase after A2780cis treated with pTC-1 for 12 hours, more than four times than those in the untreated cells. The expression level of phospho-Bad

increases slightly, and Bad remains almost constant with the treatment of pTC-1. A2780cis cells treated with pTC-1 express a high level of phosphorylated p53 and p53 over the extended incubation time, while the expression level of phosphorylated p53 slightly changes in HeLa cells.

#### Biodistribution and inhibition effect of pTC-1/TC-1 on tumor growth *in vivo*

To investigate the distribution of the assembling cholesterol derivatives in tumor-bearing murine model, we synthesized four analogues of pTC-1 that had an additional tyrosine residue for radiolabelling (by  $^{125}$ I; ref. 41; Fig. 7A). Specifically, we connect L or D enantiomer of tyrosine at N terminal of pTC-1 to form cho-p<sub>Y</sub>Y or cho-p<sub>Y</sub>Y (cho = cholesterol, p<sub>Y</sub> = D-phosphotyrosine, Y = tyrosine, and y = D-tyrosine). We also put one additional L- or D-tyrosine between cholesterol and D-phosphotyrosine, which results in cho-Y<sub>p</sub>Y and cho-y<sub>p</sub>Y, to examine the influence of indirect conjugation of cholesterol and phosphotyrosine on the cytotoxicity of the assemblies of cholesterol against A2780cis cells. The IC<sub>50</sub> values of cho-p<sub>Y</sub>Y, cho-p<sub>Y</sub>Y, cho-Y<sub>p</sub>Y, and cho-y<sub>p</sub>Y against A2780cis cells are 45, 15, 17, and 23  $\mu$ mol/L (Fig. 7B; Supplementary Fig. S11), respectively, indicating that addition of tyrosine to pTC-1 slightly lowers the cytotoxicity.

After reacting  $^{125}$ I with the tyrosine on each analogue and purifying them by high-performance liquid chromatography, we use tumor-bearing nude mice to evaluate the distribution of each of these four analogues. The results of noninvasive Gamma camera images (Fig. 7C-F) indicate that the radioactive signals are enriched in the mouse abdomen areas and the signals decrease little with extension of time, even after injection of these analogues for 96 hours (Supplementary Fig. S12). To reveal the detailed distribution of each analogue, we quantified the amounts of the pTC-1 analogues in the main organs of mice by a Gamma counter in a time-dependent manner. The results (Fig. 7G-J) indicate that the four compounds are mainly accumulated in liver, followed by blood, spleen, lung, and other organs. With increasing time, the

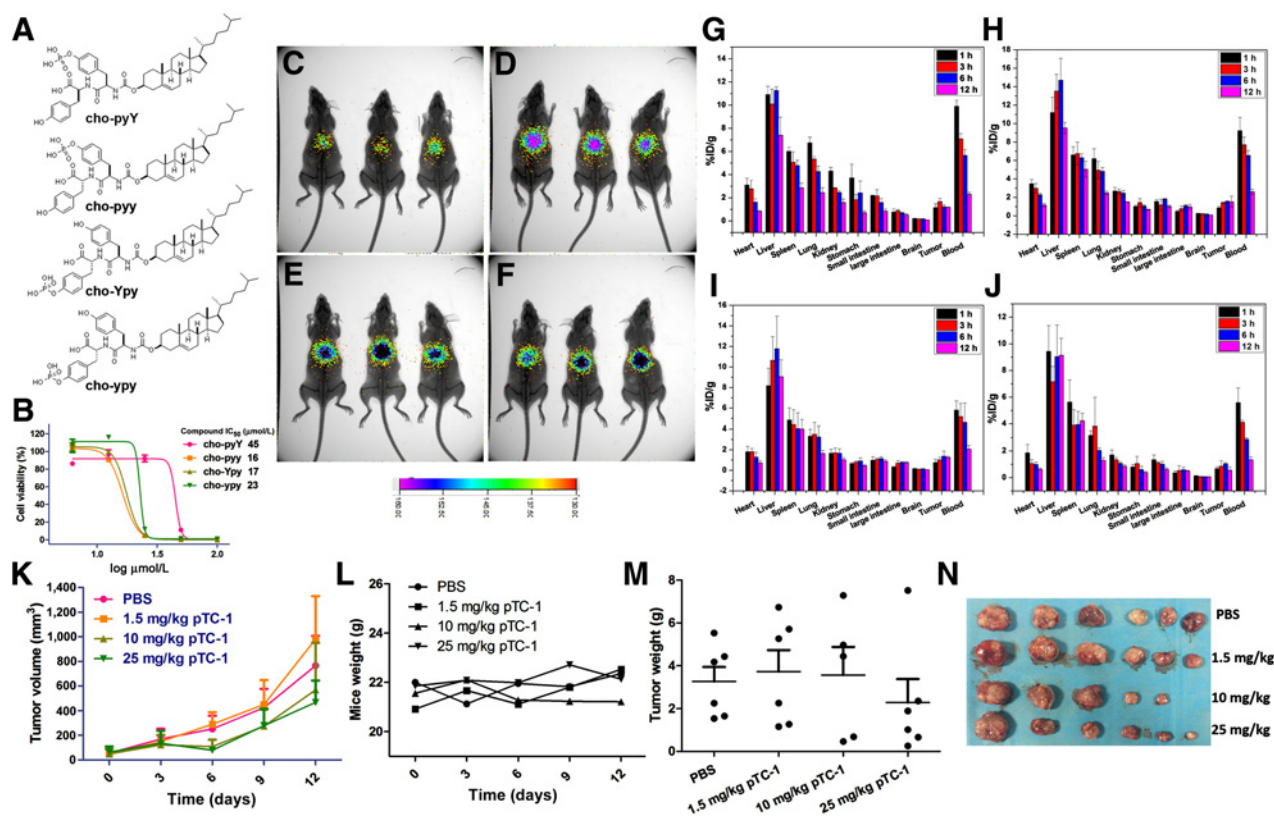


**Figure 7.**

*In vivo* distribution and tumor inhibition of the conjugates of cholesterol and tyrosine. **A**, Molecular structures of the analogues of pTC-1. **B**, Forty-eight-hour cell viability of A2780cis cell lines treated by the analogues of pTC-1 in **A**. *In vivo* noninvasive Gamma camera images of the BALB/c mice after intravenous administration with  $^{125}\text{I}$ -labeled different cholesterol derivatives cho-pyY (**C**); cho-pyy (**D**); cho-Ypy (**E**); and cho-yppy (**F**) for 12 hours, respectively. Quantitative biodistribution of  $^{125}\text{I}$ -labeled cholesterol derivatives. Tissues were harvested and weighted at 1, 3, 6, and 12 hours after initial injection of BALB/c mice, respectively. Data cho-pyY (**G**); cho-pyy (**H**); cho-Ypy (**I**); and cho-yppy (**J**) were presented as percent-injected dose per gram (%ID/g)  $\pm$  SD,  $n = 3$ . pTC-1 inhibits xenografted mouse ovarian cancer tumor (A2780cis) *in vivo* ( $n = 6$ ): the changes of tumor volume (**K**); the changes of mice weight (**L**); tumor weight after growing for 12 days (**M**); and optical images of tumors after growing for 12 days (**N**). Visual Overview: mechanism of the iA of pTC-1/TC-1 that induces cancer cell death. The up arrow indicates the upregulation of protein expression and vice versa.

radioactive signals of four analogues decrease to some extent in heart, spleen, lung, kidney, and blood.

The radioactive signals of the four analogues are different in liver. Specifically, in reference with the signal intensities at 1 hour, radioactive signals of cho-pyY decrease to 67.9% at 12 hours postinjection, while the radioactive signals of cho-pyy increase a little at first 6 hours and decrease to 84.8% at 12 hours. In contrast, the radioactive signals of cho-Ypy and cho-yppy remain almost the same at 1 hour and 12 hours. The radioactive signals of the four analogues were almost constant during tested time in large intestine and brain. Notably, the radioactive signals of cho-pyy and cho-Ypy increase a little in the tumor sites over time, agreeing that these two compounds potently inhibit A2780cis (Fig. 7B).

We then evaluate the efficacy of pTC-1 for inhibiting tumor growth in an A2780cis-bearing nude mice model. After the volume of A2780cis tumor reaches about  $50 \text{ mm}^3$ , three dosages (1.5, 10, and 25 mg/kg) of pTC-1 are intraperitoneally injected to the mice. As shown in Fig. 7K, pTC-1 efficiently inhibits the tumor growth in a dose-dependent manner at the first 6 days and delays the tumor growth in the following 6 days. Moreover, the results of

tumor weights also are consistent with the growth curve of tumors (Fig. 7M and N) in mice. These results indicate that pTC-1 inhibits the growth of the A2780cis tumors moderately. Meanwhile, we also monitored the weight changes of the mice. Our results indicate that the mice treated with pTC-1 at these three dosages have no obvious body weight loss, suggesting good *in vivo* compatibility of pTC-1.

## Discussion

This work provides molecular and cellular details of the assemblies of small molecule *in vitro* and establishes antitumor activity of the assemblies against platinum-resistant tumors *in vivo*. Cell-based screening indicate that iA of pTC-1 have more potent activity against ovarian cancer cells, which is independent to the cholesterol levels in different cell types, indicating the importance of enzymatic reaction for the cytotoxicity of iA. The less cytotoxicity of pTC-1 on HepG2 cells suggests that *in vivo* liver toxicity of pTC-1 should be low because HepG2 often acts as a model cell of hepatocyte. Our preliminary results of acquired resistance experiment indicate that pTC-1, averting resistance, likely would

minimize acquired drug resistance. The change of actin filaments in both A2780cis and HeLa cells with the increment of time, imply that iA of pTC-1 gradually disrupts the dynamics of actin filaments, which contributes to the cell death induced by pTC-1. Moreover, the changes of the morphology of mitochondria during cell death imply that the cell death involves a mitochondria-dependent apoptosis (42).

Interestingly, after the treatment with pTC-1 for 24 hours, the band of TNF-R2 disappears in both A2780cis and HeLa cells, likely is resulted from the degradation by the ubiquitin proteasome pathway. Unlike TNF-R1 that contains an intracellular death domain and can activate apoptotic pathways, TNF-R2 mediates cell survival and proliferation (43). Recent finding also revealed TNF-R2 could be a target for cancer immunotherapy (44, 45) and its upregulation could be the reason for drug resistance (46, 47). Although the reason for degradation of TNF-R2 in both A2780cis and HeLa cells remains to be addressed in future studies, the abnormal expression of TNF-R2 may contribute to the lack of acquired resistance of pTC-1 in A2780. The results of time-dependent Western blot analysis of death receptors clearly indicate that the signaling induced by pTC-1 leads to the formation of death-inducing signaling complex through the death receptors, including CD95, DR3, DR5, and TNF-R1, which further activate caspase cascade and induce cell death.

Although PERK plays an important role for adapting ER stress to cell survival during the unfolded protein response, the estimated half-life of PERK is 13 hours and it is impossible that much of the PERK expressed at one time in cells during ER stress. Moreover, under prolonged ER stress, inactivity of PERK leads to increased activity of other ER stress pathway, for example, the parallel ER stress pathways of IRE1 couple to JNKs may play key role for inducing cell death, agreeing with a previous report (48, 49). Collectively, our results clearly imply that ER stress plays crucial role in pTC-1-induced cancer cell death. That is, the ER stress activates both IRE1 and PERK branch of UPR, resulting in the activation of Bip, DR5, and Ero1 $\alpha$  to promoting CHOP expression. The cross-talks of different signaling pathways together activate caspase cascade and the related extrinsic cell death pathway, thus inducing cell death.

Finally, we use tumor-bearing murine model to see the detail distribution of pTC-1. The results indicate that pTC-1 have longer blood circulation as compared with the reported self-assembling peptides, which degrade completely after 12 hours *in vivo* (50), this result implies that doping cholesterol may provide an alternative strategy for enhancing blood circulation of therapeutic peptides. We also conduct the therapeutic activity of pTC-1 against cisplatin-resistant tumor model. The *in vivo* studies demonstrate the well biocompatibility and antitumor efficiency of pTC-1. Although antitumor efficiency of pTC-1 remains to be improved, its unprecedented ability to avert drug resistance (Supplementary Fig. S1) and to enhance the efficacy of TIC10 or

TRAIL (Fig. 5) warrants further exploration of this polypharmaceutical agent.

In summary, using an array of biochemical methods, we examined the mechanism of iA of pTC-1 that induced cancer cell death selectively. Although dying cells can release contents to induce immunogenic cell death (ICD) by relatively restricted set of stimuli, pTC-1 is unlikely to initiate ICD because it causes cell death via apoptosis. This study provides a comprehensive understanding of the signal pathways (Fig. 7, Visual Overview) involved in the cancer cell death induced by pTC-1 via enzymatically forming supramolecular assemblies (15). As a multifaceted strategy-induced cell death, iA minimizes acquired drug resistance with continuous treatment of cancer cells with pTC-1. Unlike traditional therapies which focus on targeting one specific protein or signaling pathway, this study not only highlights the advantage of therapeutic effect of iA for addressing drug resistance, but also provides a prospective method for improving the efficiency of clinical drugs. Because of a network of multiple proteins involved in one disease, the kinetics and systemic responses of cells to instructed assemblies offer new understanding on the dynamic changes of live system to molecular processes. Further exploration of the iA of small molecules as a molecular process promises novel therapeutics for cancer therapy.

#### Disclosure of Potential Conflicts of Interest

No potential conflicts of interest were disclosed.

#### Authors' Contributions

Conception and design: H. Wang, D.M. Dinulescu, B. Xu

Development of methodology: H. Wang, Z. Feng, B. Xu

Acquisition of data (provided animals, acquired and managed patients, provided facilities, etc.): H. Wang, Z. Feng, C. Yang, J. Liu, J.E. Medina, S.A. Aghvami, J. Liu, S. Fraden, B. Xu

Analysis and interpretation of data (e.g., statistical analysis, biostatistics, computational analysis): H. Wang, C. Yang, S.A. Aghvami, B. Xu

Writing, review, and/or revision of the manuscript: H. Wang, Z. Feng, B. Xu

Administrative, technical, or material support (i.e., reporting or organizing data, constructing databases): H. Wang, B. Xu

Study supervision: B. Xu

#### Acknowledgments

This work was partially supported by NIH (CA142746), NSF (DMR-1420382), and the W. M. Keck Foundation. Z. Feng thanks the Dean's Fellowship and NIH (F99CA234746). We thank Dr. D.R. Green for providing 2H18 HeLa cells.

The costs of publication of this article were defrayed in part by the payment of page charges. This article must therefore be hereby marked *advertisement* in accordance with 18 U.S.C. Section 1734 solely to indicate this fact.

Received August 31, 2018; revised October 5, 2018; accepted November 21, 2018; published first December 14, 2018.

#### References

- Stratton MR, Campbell PJ, Futreal PA. The cancer genome. *Nature* 2009; 458:719–24.
- Hudson TJ, Anderson W, Aretz A, Barker AD, Bell C, Bernabé RR, et al. International network of cancer genome projects. *Nature* 2010;464: 993–8.
- Parsons DW, Jones S, Zhang X, Lin JC, Leary RJ, Angenendt P, et al. An integrated genomic analysis of human glioblastoma multiforme. *Science* 2008;321:1807–12.
- Avendaño C, Menendez JC. Medicinal chemistry of anticancer drugs. Second edition. Elsevier Science; Boston 2015.
- Sharma P, Hu-Lieskovan S, Wargo JA, Ribas A. Primary, adaptive, and acquired resistance to cancer immunotherapy. *Cell* 2017;168: 707–23.
- Hopkins AL. Network pharmacology: the next paradigm in drug discovery. *Nat Chem Biol* 2008;4:682–90.
- Simons K, Ikonen E. How cells handle cholesterol. *Science* 2000;290:1721–6.

8. Simons K, Ikonen E. Functional rafts in cell membranes. *Nature* 1997;387:569–72.
9. Yang W, Bai Y, Xiong Y, Zhang J, Chen S, Zheng X, et al. Potentiating the antitumor response of CD8+ T cells by modulating cholesterol metabolism. *Nature* 2016;531:651–5.
10. Wang H, Feng Z, Wang Y, Zhou R, Yang Z, Xu B. Integrating enzymatic self-assembly and mitochondria targeting for selectively killing cancer cells without acquired drug resistance. *J Am Chem Soc* 2016;138:16046–55.
11. Feng Z, Wang H, Zhou R, Li J, Xu B. Enzyme-instructed assembly and disassembly processes for targeting downregulation in cancer cells. *J Am Chem Soc* 2017;139:3950–3.
12. Gao Y, Shi J, Yuan D, Xu B. Imaging enzyme-triggered self-assembly of small molecules inside live cells. *Nat Commun* 2012;3:1033.
13. Fonta C, Négyessy L, editors. *Neuronal tissue-nonspecific alkaline phosphatase (TNAP)*. the Netherlands: Springer; 2015.
14. Kuang Y, Shi J, Li J, Yuan D, Alberti KA, Xu Q, et al. Pericellular hydrogel/nanonets inhibit cancer cells. *Angew Chem Int Ed* 2014;53:8104–7.
15. Wang H, Feng Z, Wu D, Fritzsching KJ, Rigney M, Zhou J, et al. Enzyme-regulated supramolecular assemblies of cholesterol conjugates against drug-resistant ovarian cancer cells. *J Am Chem Soc* 2016;138:10758–61.
16. Nikounezhad N, Nakhjavani M, Shirazi FH. Generation of cisplatin-resistant ovarian cancer cell lines. *Iranian J Pharmac Sci* 2016;12:11–20.
17. Boldogh IR, Pon LA. Interactions of mitochondria with the actin cytoskeleton. *Biochim Biophys Acta* 2006;1763:450–62.
18. Tsai JC, Wu CL, Chien HF, Chen CT. Reorganization of cytoskeleton induced by 5aminolevulinic acid-mediated photodynamic therapy and its correlation with mitochondrial dysfunction. *Lasers Surg Med* 2005;36:398–408.
19. Estaquier J, Arnoult D. Inhibiting Drp1-mediated mitochondrial fission selectively prevents the release of cytochrome c during apoptosis. *Cell Death Differ* 2007;14:1086–94.
20. Goldstein JC, Waterhouse NJ, Juin P, Evan GI, Green DR. The coordinate release of cytochrome c during apoptosis is rapid, complete and kinetically invariant. *Nat Cell Biol* 2000;2:156.
21. Koh CH, Cheung NS. Cellular mechanism of U18666A-mediated apoptosis in cultured murine cortical neurons: bridging Niemann–Pick disease type C and Alzheimer's disease. *Cell Signal* 2006;18:1844–53.
22. Ashkenazi A, Salvesen G. Regulated cell death: signaling and mechanisms. *Annu Rev Cell Dev Biol* 2014;30:337–56.
23. Shatnyeva OM, Kubarenko AV, Weber CE, Pappa A, Schwartz-Albiez R, Weber AN, et al. Modulation of the CD95-induced apoptosis: the role of CD95 N-glycosylation. *PLoS One* 2011;6:e19927.
24. Lu M, Lawrence DA, Marsters S, Acosta-Alvear D, Kimmig P, Mendez AS, et al. Opposing unfolded-protein-response signals converge on death receptor 5 to control apoptosis. *Science* 2014;345:98–101.
25. Yamaguchi H, Wang HG. CHOP is involved in endoplasmic reticulum stress-induced apoptosis by enhancing DR5 expression in human carcinoma cells. *J Biol Chem* 2004;279:45495–502.
26. Tabas I, Ron D. Integrating the mechanisms of apoptosis induced by endoplasmic reticulum stress. *Nat Cell Biol* 2011;13:184.
27. Zlotorynski E. Apoptosis: DR5 unfolds ER stress. *Nat Rev Mol Cell Biol* 2014;15:498.
28. Feng B, Yao PM, Li Y, Devlin CM, Zhang D, Harding HP, et al. The endoplasmic reticulum is the site of cholesterol-induced cytotoxicity in macrophages. *Nat Cell Biol* 2003;5:781.
29. Ron D, Walter P. Signal integration in the endoplasmic reticulum unfolded protein response. *Nat Rev Mol Cell Biol* 2007;8:519.
30. Harding HP, Zhang Y, Ron D. Protein translation and folding are coupled by an endoplasmic-reticulum-resident kinase. *Nature* 1999;397:271.
31. Delom F, Emadali A, Cocolakis E, Lebrun J, Nantel A, Chevet E. Calnexin-dependent regulation of tunicamycin-induced apoptosis in breast carcinoma MCF-7 cells. *Cell Death Differ* 2007;14:586.
32. Takizawa T, Tatematsu C, Watanabe K, Kato K, Nakanishi Y. Cleavage of calnexin caused by apoptotic stimuli: implication for the regulation of apoptosis. *J Biochem* 2004;136:399–405.
33. Zhang S, Yu D. Targeting Src family kinases in anti-cancer therapies: turning promise into triumph. *Trends Pharmacol Sci* 2012;33:122–8.
34. Kim LC, Song L, Haura EB. Src kinases as therapeutic targets for cancer. *Nat Rev Clin Oncol* 2009;6:587.
35. Mayer EL, Krop IE. Advances in targeting SRC in the treatment of breast cancer and other solid malignancies. *Clin Cancer Res* 2010;16:3526–32.
36. Manek R, Pakzamid E, Mhawech-Fauceglia P, Pejovic T, Sowter H, Gayther SA, et al. Targeting Src in endometriosis-associated ovarian cancer. *Oncogenesis* 2016;5:e251.
37. Chen Z, Oh D, Dubey AK, Yao M, Yang B, Groves JT, et al. EGFR family and Src family kinase interactions: mechanics matters? *Curr Opin Cell Biol* 2018;51:97–102.
38. Allen JE, Krigsfeld G, Mayes PA, Patel L, Dicker DT, Patel AS, et al. Dual inactivation of Akt and ERK by TIC10 signals Foxo3a nuclear translocation, TRAIL gene induction, and potent antitumor effects. *Sci Transl Med* 2013;5:171ra17.
39. Nair PM, Flores H, Gogineni A, Marsters S, Lawrence DA, Kelley RF, et al. Enhancing the antitumor efficacy of a cell-surface death ligand by covalent membrane display. *Proc Natl Acad Sci U S A* 2015;112:5679–84.
40. Wang S, Ren W, Liu J, Lahat G, Torres K, Lopez G, et al. TRAIL and doxorubicin combination induces proapoptotic and antiangiogenic effects in soft tissue sarcoma in vivo. *Clin Cancer Res* 2010;16:2591–604.
41. Buchsbaum DJ, Walker PC, Johnson EA. Distribution of radiolabeled alloantibodies in mice bearing 3-methylcholanthrene-induced sarcomas. *Cancer Res* 1979;39:3363–8.
42. Frank S, Gaume B, Bergmann-Leitner ES, Leitner WW, Robert EG, Catez F, et al. The role of dynamin-related protein 1, a mediator of mitochondrial fission, in apoptosis. *Dev Cell* 2001;1:515–25.
43. Aggarwal BB. Signalling pathways of the TNF superfamily: a double-edged sword. *Nat Rev Immunol* 2003;3:745.
44. Torrey H, Butterworth J, Mera T, Okubo Y, Wang L, Baum D, et al. Targeting TNFR2 with antagonistic antibodies inhibits proliferation of ovarian cancer cells and tumor-associated Tregs. *Sci Signal* 2017;10:eaaf8608.
45. Vanamee ES, Faustman DL. TNFR2: a novel target for cancer immunotherapy. *Trends Mol Med* 2017;23:1037–46.
46. Zhao T, Li H, Liu Z. Tumor necrosis factor receptor 2 promotes growth of colorectal cancer via the PI3K/AKT signaling pathway. *Oncol Lett* 2017;13:342–6.
47. Yang F, Zhao N, Wu N. TNFR2 promotes adriamycin resistance in breast cancer cells by repairing DNA damage. *Mol Med Rep* 2017;16:2962–8.
48. Harding HP, Zhang Y, Bertolotti A, Zeng H, Ron D. Perk is essential for translational regulation and cell survival during the unfolded protein response. *Mol Cell* 2000;5:897–904.
49. Bertolotti A, Zhang Y, Hendershot LM, Harding HP, Ron D. Dynamic interaction of BiP and ER stress transducers in the unfolded-protein response. *Nat Cell Biol* 2000;2:326.
50. Yang C, Chu L, Zhang Y, Shi Y, Liu J, Liu Q, et al. Dynamic biostability, biodistribution, and toxicity of L/D-peptide-based supramolecular nanofibers. *ACS Appl Mat Interf* 2015;7:2735–44.

# Molecular Cancer Research

## Unraveling the Cellular Mechanism of Assembling Cholesterols for Selective Cancer Cell Death

Huaimin Wang, Zhaoqianqi Feng, Cuihong Yang, et al.

*Mol Cancer Res* 2019;17:907-917. Published OnlineFirst December 14, 2018.

**Updated version** Access the most recent version of this article at:  
doi:[10.1158/1541-7786.MCR-18-0931](https://doi.org/10.1158/1541-7786.MCR-18-0931)

**Supplementary Material** Access the most recent supplemental material at:  
<http://mcr.aacrjournals.org/content/suppl/2018/12/13/1541-7786.MCR-18-0931.DC1>

**Visual Overview** A diagrammatic summary of the major findings and biological implications:  
<http://mcr.aacrjournals.org/content/17/4/907/F1.large.jpg>

**Cited articles** This article cites 48 articles, 10 of which you can access for free at:  
<http://mcr.aacrjournals.org/content/17/4/907.full#ref-list-1>

**E-mail alerts** [Sign up to receive free email-alerts](#) related to this article or journal.

**Reprints and Subscriptions** To order reprints of this article or to subscribe to the journal, contact the AACR Publications Department at [pubs@aacr.org](mailto:pubs@aacr.org).

**Permissions** To request permission to re-use all or part of this article, use this link  
<http://mcr.aacrjournals.org/content/17/4/907>.  
Click on "Request Permissions" which will take you to the Copyright Clearance Center's (CCC) Rightslink site.